Digital Discovery

ROYAL SOCIETY OF CHEMISTRY

PAPER

View Article Online
View Journal | View Issue

Cite this: *Digital Discovery*, 2025, **4**, 2491

AMPERE-2: an open-hardware, robotic platform for automated electrodeposition and electrochemical validation

Nis Fisker-Bødker, †*[a] Daniel Persaud, †[b] Yang Bai, *[c] Mark Kozdras,[d] Tejs Vegge,[a] Jason Hattrick-Simpers[b] and Jin Hyun Chang *[a]

An Opentrons OT-2 liquid-handling robot was used as the framework to develop an automated platform for the electrodeposition and electrochemical testing of multi-element catalysts. Catalytic activity was demonstrated *via* alkaline water splitting, specifically targeting the oxygen evolution reaction (OER). The setup integrates multiple pumps, a flushing tool, custom deposition and electrochemical testing electrodes, and a potentiostat to enable reproducible and efficient electrodeposition and evaluation. Stock solutions of metal chlorides were combined with two complexing agents, ammonium hydroxide and sodium citrate, to stabilize the deposition process and tune the surface morphology. Analysis by cyclic voltammetry and electron microscopy revealed that the complexing agents significantly influenced deposition rates and surface structures, with the most effective catalysts forming either in the absence of additives or when both agents were applied together. Deposition times of 30–60 seconds yielded the lowest OER overpotentials, indicating an optimal catalyst layer thickness. The platform demonstrates robust reproducibility with uncertainty in overpotential measurements at 16 mV.

Received 1st May 2025
Accepted 20th July 2025

DOI: 10.1039/d5dd00180c

rsc.li/digitaldiscovery

1 Introduction

The increasing adoption of self-driving laboratories (SDLs) is revolutionizing materials discovery across multiple fields. These robotic platforms, integrated with artificial intelligence (AI), autonomously execute and optimize experimental workflows, enabling researchers to explore vast material search spaces while rapidly testing and evaluating multiple material compositions and experimental conditions.[1,2] In 2022, the Clio flow-through robot exemplified how closed-loop optimization can uncover fast-charging Li-ion electrolyte formulations in fewer than fifty experiments.[3] In another experiment a liquid-handling robot was used to optimize solid-polymer-electrolytes for Li-batteries.[4] The capability for rapid manufacturing, inline evaluation, and optimization are particularly valuable in catalyst design, where discovering new catalysts requires navigating complex multicomponent systems and identifying promising candidates from large experimental sequences.[5–9] Autonomous electrochemistry has likewise advanced battery materials discovery; for example, Sanin *et al.*[10] deployed a scanning-droplet-cell robot to map over 1000 Si–Ge–Sn thin-film anode compositions in closed loop with machine learning.

Despite their potential, the widespread adoption of SDLs is hindered by high costs and technical complexity. State-of-the-art platforms require substantial financial investment and demand interdisciplinary expertise spanning mechanical and electrical engineering, software development, chemistry, and AI.[11–14] Existing robotic liquid-handling systems fall into three categories: do-it-yourself (DIY) setups, modifiable off-the-shelf robotic systems, and fully customized commercial platforms. While affordable DIY options, such as the ~150 USD platform by Li *et al.*[15] and the LEGO-based system by Gerber *et al.*,[16] offer low-cost entry points, they often lack the robustness and scalability required for advanced research applications. Bai *et al.*[17] combined a custom DIY platform with higher-end off-the-shelf instrumentation for the fabrication and characterization of electrocatalytic materials. Off-the-shelf robotic systems, such as the Beckman Biomek i5, Eppendorf Epmotion 5075, and Opentrons OT-2, provide greater reliability and reproducibility but require customization to meet specific research needs.

In this work, we selected the widely used Opentrons OT-2 platform due to its open-source nature, affordability, and accessibility, which support collaboration among research groups capable of 3D printing custom components and ordering customized parts. This approach helps to democratize

[a]*Department of Energy Conversion and Storage, Technical University of Denmark, Anker Engelundsvej 101, 2800 Kgs Lyngby, Denmark. E-mail: nisfi@dtu.dk; jchang@dtu.dk*

[b]*Department of Materials Science and Engineering, University of Toronto, 184 College Street, Toronto, Ontario M5S 3E4, Canada*

[c]*Accelerate Consortium, University of Toronto, 80 St. George St., Toronto, ON M5S 3H6, Canada. E-mail: yangb.bai@utoronto.ca*

[d]*CanmetMaterials, Natural Resources Canada, Hamilton, ON, Canada*

† Nis Fisker-Bødker and Daniel Persaud contributed equally to this work.

SDL by lowering the barrier to entry.[18] In contrast, fully customized commercial systems, while potentially reducing engineering effort, can hinder federated inter-laboratory collaboration due to proprietary restrictions and reliance on specialized expertise for maintenance and modifications. The high cost and steep learning curve associated with these systems present challenges for broader SDL adoption.[19]

We developed an automated platform designed to democratize access to SDLs by reducing technical barriers and offering a cost-effective solution for practical applications in materials science. Inspired by the previously reported Automated Modular Platform for Expedited and Reproducible Electrochemical testing (AMPERE),[20] a new, fully automated AMPERE-2 seamlessly integrates material synthesis *via* automated electrodeposition with immediate electrochemical evaluation, eliminating the need for human intervention. Similar closed-loop studies have used electrodeposition to optimize Co–Fe–Mn mixed-metal oxides for acidic OER, highlighting the experimental noise challenges associated with autonomous electrochemical workflows.[21]

The oxygen evolution reaction (OER) overpotential refers to the excess voltage required beyond the thermodynamic minimum of 1.23 V to drive water splitting. It is a critical performance metric for electrocatalysts and a common target for machine learning-based optimization.[8] Automated voltammetric interrogation of reaction mechanisms has recently been demonstrated in an autonomous flow-cell that collected over 2500 cyclic voltammograms without human intervention, underscoring the value of closed-loop electrochemical analytics.[22] AMPERE-2 successfully demonstrates a fully autonomous workflow for catalyst synthesis and OER evaluation in this study. As a benchmark, $NiFeO_x$ and NiO_x were synthesized and evaluated, achieving performance consistent with literature values and confirming the platform's experimental reproducibility. Furthermore, a novel NiFeCrMnCoZnCu alloy was synthesized and evaluated, achieving an overpotential at current density of 50 mA cm^{-2} (η_{50}) of 451 mV for alkaline OER, outperforming NiO_x (η_{50} = 731 mV) in catalytic activity. By lowering the financial and technical barriers, AMPERE-2 facilitates broader exploration of multi-element systems, such as corrosion-resistant materials and electrocatalysts, thereby accelerating progress in electrochemical energy research.

2 Experimental setup

The Opentrons OT-2 platform provides a robust foundation for laboratory automation, offering built-in liquid handling capabilities that simplify the development of advanced workflows. By leveraging this existing functionality and incorporating standardized protocols for electrodeposition and electrochemical testing, full automation can be achieved without the need for extensive engineering or costly custom equipment.

Building on the OT-2 system, the AMPERE-2 platform extends its capabilities to enable automated catalyst synthesis and electrochemical characterization (Fig. 1). AMPERE-2 integrates custom hardware components for electrodeposition, electrochemical testing, cleaning, and temperature control of the reaction chamber. The platform features a deck layout (Fig. 1a) designed to hold cartridges for storing customized tools, reagents, and pipette tips, as well as wells for synthesis, testing, and cleaning. Arduino-controlled electronics are integrated into the platform to manage fluid handling, ultrasonic mixing, and temperature regulation.

2.1 Customized functional tools

A set of tools, as shown in Fig. 1c–f, were crafted to improve the OT-2's functionality. The tools are engineered with tips modeled after a 1000 μL pipette tip, enabling the electric OT-2 P1000 pipette to engage and disengage the tools in a manner identical to the handling of standard pipette tips. These tools are stored in a tool rack cartridge shown in Fig. 1a (labeled 1).

The electrodeposition electrode shown in Fig. 1c consists of a Ø10 mm nickel rod connected to a potentiostat (labeled 8 in Fig. 1b) *via* a cable. This electrode can be substituted with alternative materials, such as a carbon rod or platinum, to accommodate various electrochemical processes during electrodeposition.

A two-electrode configuration tool is designed to accommodate various electrochemical testing needs. Fig. 1d shows the first option; an Ag/AgCl reference electrode assembly (CH Instruments, CHI103) integrated with a Ø0.25 mm platinum wire counter electrode (CE) wrapped around the glass shaft. This compact design is optimized for narrow wells (∼Ø10 mm), enabling precise electrochemical measurements in confined reaction environments. The second option that combines a reversible hydrogen electrode (RHE) (Mini Hydroflex by Gaskatel) and a 1 cm × 1 cm × 1 mm platinum plate serving as CE is shown in Fig. 1e. The placement of the RHE determines the geometry of the well during testing.

The flush tool used for cleaning the reactor before and after experiments (Fig. 1f) was fabricated using a Formlabs Form 4 resin printer with chemically resistant Draft v2 resin. The OT-2 is a liquid-handling platform and can in principle perform the same task using three pipettes. If pipettes are used, it takes around 15 minutes for each of the three cleaning rounds. In contrast, the flush tool completes a flush cycle in around 1 minute, saving approximately 42 minutes per experiment and enabling continuous flow, which is more effective for cleaning than pipetting alone.

Unlike the flush tool, the other custom tools can be printed using any standard resist or filament since they do not come into contact with reactive liquids. The flush tool features a conical geometry with a drainage opening at the tip, enabling efficient removal of liquids and suspended solids following chemical processing. To enhance cleaning efficiency, two side apertures allow controlled delivery of water and acid into the reaction chamber. The tool is connected through silicone tubing to three peristaltic pumps and associated chemical reservoirs (label 7 in Fig. 1b).

Cable socks are wrapped around all cables coming out of the functional tools to prevent cables and tubes from tangling during tool movement. Zip ties are used to guide the socks by fastening them to provide sufficient rigidity, allowing them to

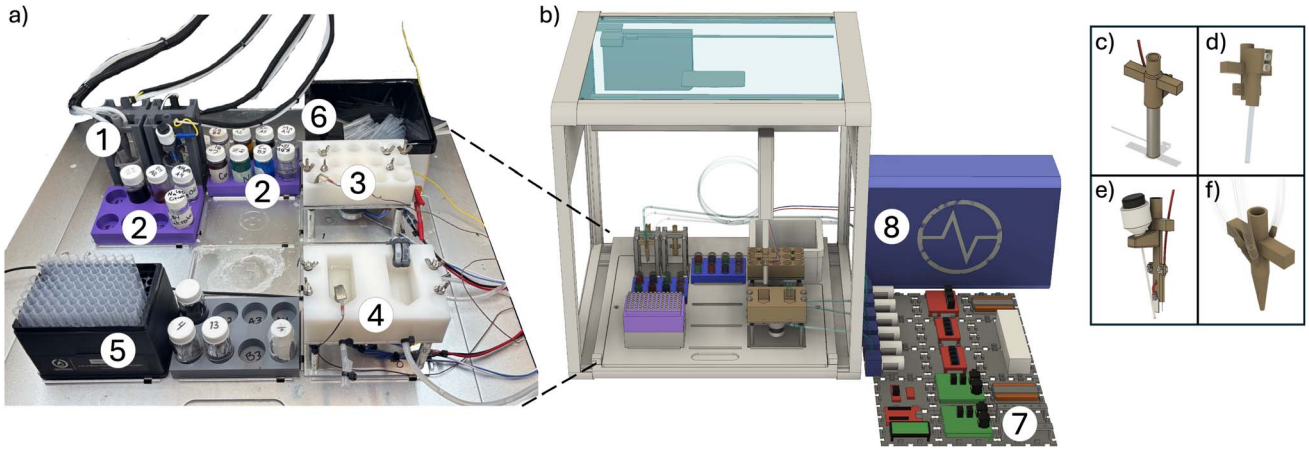

Fig. 1 (a) Deck layout of OT-2 platform used in this study. (b) 3D model of the OT-2 platform, showing the robot and fully assembled setup. (c) Ni deposition electrode; (d) Ag/AgCl reference electrode paired with a platinum (wire) electrode; (e) RHE and 2 cm^2 platinum CE; (f) flush tool for cleaning; labeled components of the platform: (1) tool rack cartridge holding four tools shown in c–f, (2) vial cartridge for storing reagents, (3) array reactor cartridge, where synthesis and testing are conducted, mounted on a base with heating and ultrasound capabilities, (4) cleaning cartridge, mounted on a base with heating and ultrasound, used to clean tools after use, (5) cartridge holding pipette tips for precise liquid handling, (6) waste bucket for discarded pipette tips, (7) peristaltic pumps, their reservoirs, Arduino controller, heat sensors, and other electronics, (8) potentiostat for electrochemical measurements.

hover over the components of the robotic deck, as shown in Fig. 1a.

2.2 Array reactor and cleaning bath

The array reactor, shown in Fig. 2, serves as a reaction chamber for both electrodeposition and electrochemical testing, employing a bottom-of-the-well working-electrode concept similar to the self-driving platform for polymer-film electrodeposition by Quinn *et al.*[23] Designed to accommodate high-throughput experiments, the array reactor consists of 15 cone-shaped wells, each providing a controlled environment for alloy synthesis and evaluation. A thermocouple is mounted in one of the 15 wells to monitor the temperature throughout the experiment. In this study, the total number of wells was 15, but this can be increased by duplicating the array reactor and its base, allowing for up to 90 wells. Increasing the number of wells would require additional stock solution volume and supplementary temperature control electronics, both of which are feasible extensions of the current system.

The array reactor is constructed by CNC machining a 30 mm thick High-Density Polyethylene (HDPE) block with 15 cone-shaped wells, which act as a reaction chamber for the electrochemical experiments. Each conical well has a top diameter of Ø20 mm and a bottom diameter of Ø4 mm. The conical shape was chosen to minimize the solution volume to 3.9 mL while accommodating large experimental tools. The bottom diameter of Ø4 mm in the conical wells yields an approximate surface area of the working electrode to be around 0.2827 cm^2. An O-ring is placed and compressed between the HDPE and nickel foil to ensure a tight seal and a leak-proof environment. The reactor top is secured with headed screws and wing nuts, ensuring a reliable seal. A 3 mm-thick aluminum plate coated with a 0.5 mm nickel foil layer acts as a robust and conductive support, as shown in Fig. 2a. Since the cartridge base is connected to a potentiostat as the working electrode (WE), the nickel foil serves as the WE in this configuration.

A cartridge base was developed to extend the capabilities of the array reactor. As shown in Fig. 2b, the base is constructed with four aluminum columns separating two aluminum decks: the lower deck is designed to fit securely in the OT-2's deck slot, while the upper deck accommodates interchangeable modules such as the array reactor. The base contains a 50 W ultrasonic transducer operating at 44 kHz and two 110 VAC, 17 W heating elements that automatically shut down at 100 °C. These components enhance solution mixing during reactions and facilitate thorough cleaning of the reactor and electrodes. The fixation of the array reactor to the base is achieved using wing

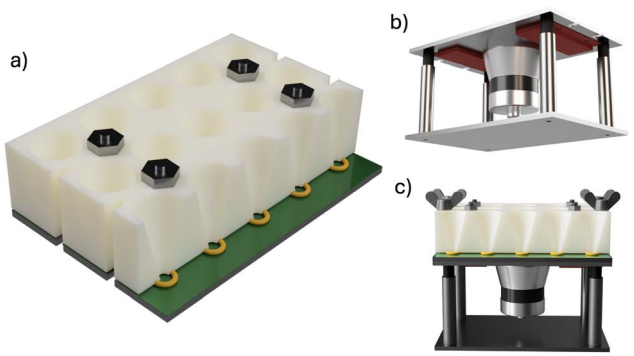

Fig. 2 (a) Cross-sectional view of the array reactor, displaying the cone-shaped wells and nickel foil (green) functioning as the working electrode, separated by a yellow silicone O-ring to ensure a sealed interface. (b) Base cartridge equipped with ultrasound, heating elements, and rubber dampeners for vibration absorption. (c) Side view of the array reactor mounted onto the base cartridge, which also supports the mounting of the cleaning bath.

nuts and screws, as illustrated in Fig. 2c, which ensures a stable and secure attachment.

The heating elements operate *via* pulse width modulation (PWM) controlled by a SparkFun Qwiic Dual Solid State Relay to regulate power delivery. The ultrasonic transducer is managed through a SparkFun Qwiic Quad Relay in combination with a dedicated driver. A 8 mm diameter rubber dampener is installed on each corner rod to minimize vibrations in the setup. The base is designed for easy integration with both the array reactor and the cleaning bath (label 7 in Fig. 1a), featuring side slots on the top plate that allow for straightforward and secure installation. The surface of the base acts as a conductive element for the working electrode during electrodeposition and electrochemical testing. To maintain continuous electrical connectivity, a nickel-coated terminal lug is positioned beneath the upper deck to ensure direct contact with both the rubber dampener and the aluminum plate.

The cleaning bath was designed to enable automated electrode cleaning between experimental runs to prevent cross-contamination. Machined from HDPE, the station is a combination of various cleaning solutions, including water and acid, depending on the specific requirements of the experiment. When positioned on the cartridge base, the cleaning bath benefits from both ultrasound and temperature control to enhance the removal of residue and ensure thorough cleaning. During the automated workflow, the electric pipette on the OT-2 moves tools into the cleaning bath after experimental processes such as electrodeposition and electrochemical testing, where an efficient and thorough cleaning protocol is performed. The bath incorporates a side port connected to a peristaltic pump to enable automated drainage of the cleaning solution. The sloped design of the cartridge base directs loose particles toward the drain, ensuring effective removal of contaminants between cycles (Fig. S10).

2.3 Electronic control system

To extend the functionality of the OT-2 robotic system, additional hardware components were integrated to enable automated fluid handling, temperature control, and ultrasonic mixing (label 7 in Fig. 1b). The control system is built around a SparkFun Arduino Uno RedBoard with a Qwiic connection, providing easy integration of I2C-compatible components for real-time system control and management. The setup includes six 12 VDC peristaltic pumps, two 110 VAC 50 W ultrasonic drivers and transducers, and four 110 VAC 17 W heating elements. All printed circuit boards (PCBs) and pumps are mounted on custom 3D-printed tiles designed for a snap-together assembly, allowing for straightforward upgrades and replacements.

To prevent the Arduino from rebooting upon establishing a USB serial connection, a 10 μF capacitor was placed between the RESET and GND pins. However, this capacitor must be temporarily removed when uploading new firmware to the board. Each peristaltic pump is controlled *via* a relay and powered by the 12 VDC power supply, allowing independent fluid control. The ultrasonic transducers receive power through relays to enable controlled activation and deactivation. The heating elements are regulated by two solid-state relays operating at 120 Hz. Temperature control is achieved through PWM and a Proportional-Integral-Derivative (PID) controller on the Arduino, which dynamically adjusts power output based on real-time feedback from the thermocouples. Each peristaltic pump was calibrated using an analytical scale and tested with its final tubing configuration to compensate for resistance and flow rate variations (details in (SI) in Table S3 and Fig. S12). This integrated hardware system enhances automation, improves reproducibility, and ensures consistent experimental conditions.

The connections between each component are illustrated in Fig. 3a, showing the integration of the potentiostat, the electrode tools, and the pump system. The potentiostat is connected to all electrode tools (Fig. 1c–e), which are all configured as a CE. While all CEs are charged and active, only the electrode tool physically immersed in the solution with the reaction chamber completes the electrical circuit and thus contributes to the electrochemical measurement. A relay connected to the potentiostat's reference lead controls which reference electrode is engaged during operation. During electrodeposition, the relay routes the signal to measure between the CE and WE to enable absolute potential control. During electrochemical testing, the measurement is switched to WE *versus* the reference electrode (RHE or Ag/AgCl, depending on the tool in use), allowing for relative potential measurements under standard conditions.

The pump system is designed to automate the flushing and cleaning processes. The flush tool is connected *via* silicone tubing to peristaltic pumps: one drains liquid from the reaction chamber through the tip of the tool, another supplies acid for cleaning, and the third delivers water for flushing. Additional pumps are dedicated to the cleaning bath, supplying water and acid for clean tools immersed in the bath, and one pump handles waste removal by draining the bath after use. One cleaning bath remained unused in the current experimental setup, but can be integrated in future expansion. This configuration enables precise fluid handling, ensuring efficient cleaning and preventing cross-contamination between experiments.

2.4 Software

The software structure governing the experimental automation process is shown in Fig. 3b. The *main.py* script loads all classes as objects and defines the variables in the experimental recipe. These variables include the chemical composition of metals and complexing agents, as well as temperature, time, flushing chemicals, and ultrasound usage. The user can either select an AI-driven optimizer or manually input a predefined list of experiments in *main.py*.

The overall workflow is managed by *experiment.py*, which orchestrates the sequence of operations and hardware signals. This script interfaces with *ardu.py*, which communicates with the Arduino to control key functions such as activating and deactivating peristaltic pumps, ultrasound, temperature

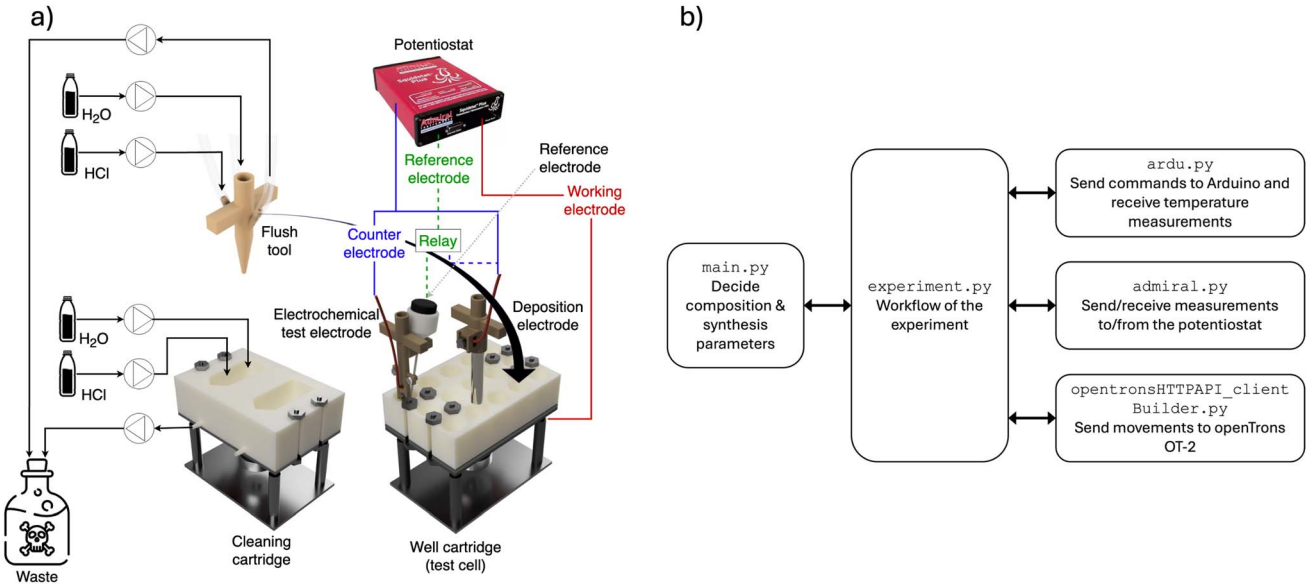

Fig. 3 (a) Schematic of the AMPERE-2 electrodeposition setup, showing the connection between the potentiostat, pumps, and functional tools. (b) Overview of software structure: *main.py* initializes the workflow by setting experimental parameters such as temperature, deposition current, and metal precursor combinations. These parameters are passed to *experiment.py*, which coordinates control of Arduino, potentiostat, and OT-2.

stabilization, and temperature measurement. Cartridges and tools are configured through JSON files and loaded *via opentronsHTTPAPI_clientBuilder.py*, which also transmits movement instructions to the OT-2 liquid-handling robot. This setup allows the OT-2 to execute dynamic tasks, such as pausing and hovering over a chamber in the array reactor during flushing or electrochemical measurements. Such flexibility is not achievable using Opentrons' standard recipe-uploading software, which restricts the integration of external tools beyond the OT-2 framework. Finally, *admiral.py* interfaces with the Admiral Squidstat Plus potentiostat, collecting electrochemical measurement data, which is then saved in CSV format for further analysis.

3 Alloy synthesis *via* electrodeposition

The incorporation of first–row transition metal ions (Fe^{3+}, Cr^{3+}, Co^{2+}, Ni^{2+}, Mn^{2+}, Zn^{2+}, Cu^{2+}) into nickel-based catalysts has attracted significant attention for enhancing OER performance in alkaline media.[24,25] These metals offer earth-abundant and cost-effective alternatives to platinum group metals (PGMs) and provide tunable electronic structures that can synergistically interact with nickel to improve catalytic activity.[26,27] For instance, Fe^{3+} and Co^{2+} have been shown to promote the formation of higher oxidation states in nickel, facilitating charge transfer and boosting OER efficiency.[26,28] Although some metals, such as Mn^{2+} and Cu^{2+}, can suppress OER activity due to unfavorable electronic configurations or redox behaviors, strategic alloying and optimization can yield catalysts with enhanced performance and stability.[29,30] Electrodeposition provides a straightforward synthesis route for such multimetallic catalysts, making it particularly well-suited for robotic and automated applications.

Stock solutions of 0.4 M concentration were prepared from a selection of metal salts, namely $NiCl_2$ (≥98% purity), $FeCl_3$ (≥97% purity), $CrCl_2 \times 6H_2O$ (≥98% purity), $MnCl_2$ (≥99% purity), $CoCl_2$ (≥97% purity), $ZnCl_2$ (≥98% purity), and $CuCl_2$ (≥97% purity). These salts were supplied by Sigma-Aldrich. Each salt was dissolved in deionized water with stirring, followed by the addition of 37 wt% HCl until the pH reached 2.0. This process ensured that each stock solution was clear and free of precipitates or turbidity.

The electrodeposition process was stabilized using two complexing agents: 30 wt% NH_4OH, with a quality level of 200, and $Na_3C_6H_5O_7$, with a purity of ≥99%, both sourced from Sigma-Aldrich. The use of complexing agents has been reported to significantly impact reaction rates as well as alter the surface structure and composition.[31–33] In line with the methodologies outlined in ref. 32 and 33, sodium citrate was dissolved in water at a concentration of 0.5 M, where it was used as a complexing agent.

For simplicity, the equivolumetric mixture of metal stock solutions used in this study is referred to as NFCMCZC, which represents a combination of Ni, Fe, Cr, Mn, Co, Zn, and Cu chloride solutions. In the absence of complexing agents, NFCMCZC corresponds to the following volume-based compositions: $Ni_{0.14}Fe_{0.14}Cr_{0.14}Mn_{0.14}Co_{0.14}Zn_{0.14}Cu_{0.14}$, indicating that each metal contributes 14% of the total solution volume. When both complexing agents are incorporated, the mixture is denoted as NFCMCZC + Am + Ci, where Am represents ammonium hydroxide (NH_4OH) and Ci denotes sodium citrate ($Na_3C_6H_5O_7$). In this case, the volume distribution becomes: $Ni_{0.11}Fe_{0.11}Cr_{0.11}Mn_{0.11}Co_{0.11}Zn_{0.11}Cu_{0.11}$ + $(Na_3C_6H_5O_7)_{0.11}$ +

$(NH_4OH)_{0.11}$. Analogous naming conventions are used for formulations containing only one of the two complexing agents.

A 1 M KOH solution (Thermo Scientific) was used as the electrolyte for subsequent alkaline water-splitting experiments and OER catalyst testing. The solution was used as received without pre-electrolysis or filtration to remove trace metals such as Fe species, which are known to enhance the OER activity artificially.[34]

3.1 Automated workflow

All metal solutions, complexing agents, and the KOH electrolyte were placed in 20 mL vials and loaded into the vial cartridge (labeled 2 in Fig. 1a). The vials were uncapped before the experiment and left open for the following ~16 hours (15 samples in an array, each taking approximately 65 minutes). For longer experiments or when using more volatile reagents, evaporation could become significant. In such cases, capped vials with rubber septa or similar sealing strategies would be recommended. The experiment was executed using a custom Python wrapper for the Opentrons API and a dedicated interface for the Admiral potentiostat. The detailed step-by-step protocol is available in the SI, and all control codes, including the Arduino scripts, are available in the Data availability section.

Fig. 4 illustrates the automated workflow, which begins by setting the experiment parameters and heating the reactor to 35 C to enhance the deposition rate. The reactor is then pre-cleaned using the flush tool: two water rinses are followed by 5 seconds of ultrasound, a hydrochloric acid rinse with 30 seconds of ultrasound, and two final water rinses with 5 seconds of ultrasound. This ensures a clean nickel substrate before deposition.

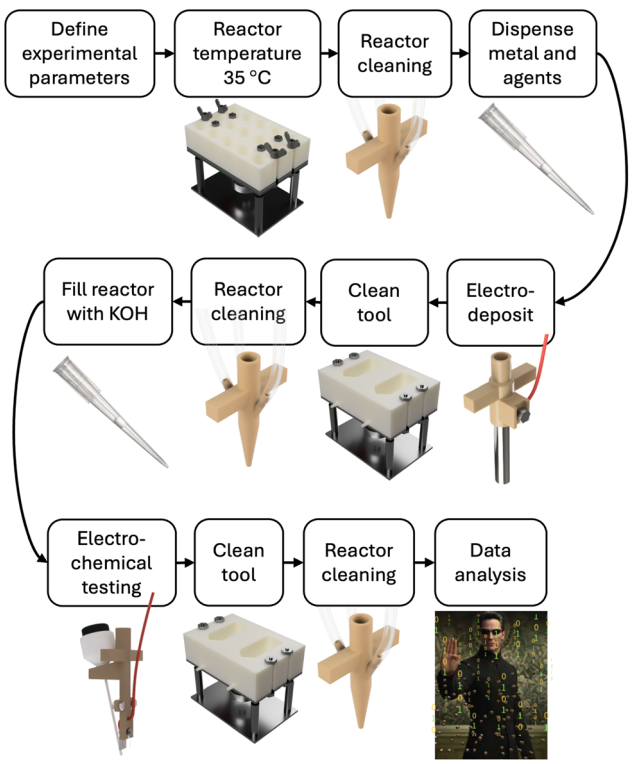

Fig. 4 Overview of the automated workflow implemented in the AMPERE-2 platform. After defining experiment parameters, the system autonomously executes the reagent dosing, electrodeposition, electrochemical testing (CV, EIS, and CC), and tool cleaning. The final output includes the overpotential value, which can be used directly in optimization routines.

Metal solutions and complexing agents are dispensed in the specified ratios using individual pipettes. Electrodeposition is carried out using the electrodeposition tool at a constant current density of 10 mA cm^{-2} for 60 seconds. After deposition, the tool is cleaned with HCl, water, and ultrasound in the cleaning cartridge. The reactor is then emptied and flushed again using the flush tool, omitting the ultrasound during the HCl rinse. Subsequently, it is filled with 1 M KOH *via* a pipette for electrochemical testing. The electrochemical test tool equipped with RHE is inserted, and the system performs cyclic voltammetry (CV), electrochemical impedance spectroscopy (EIS), and constant current (CC) measurements. Following testing, the tool undergoes the same cleaning procedure. Finally, the reactor is rinsed once more using two water flushes with 5 seconds of ultrasound applied to each. Data from the electrochemical measurements are then analyzed to determine the overpotential of the catalyst for the OER, enabling a direction integration into Bayesian optimization routines.

The run-time for each well in the array reactor is approximately 65 minutes, including all steps (initial sample cleaning, electrodeposition, electrochemical testing, and final cleaning). With the current protocol, up to 22 samples can be processed per day. Current electrochemical testing routines include CV, CP, and EIS, with a total duration of approximately 40 minutes. These routines can be adjusted as needed, which would influence both the testing time per sample and the overall throughput of the system.

3.2 Limiting current analysis

To estimate the limiting current for each individual metal solution, CV scans were conducted from +0.5 V to – 10 V and back to +0.5 V, measured *versus* CE. These scans were performed prior to electrodeposition. The downward sweep, shown in part in Fig. 5a, illustrates the deposition behavior of each metal. The onset of the Hydrogen Evolution Reaction (HER) is expected near −1.23 V, while the Chlorine Evolution Reaction (CER) occurs around −1.36 V.[35]

The four methods outlined by Ponce-De-León *et al.*[36] for determining the limiting current proved difficult to apply to the experimental data due to signal noise. Instead, the limiting current was approximated by extracting the current density at −1 V, prior to H_2 or Cl_2 gas evolution. This value was used as a proxy for the limiting current density. Among the tested single metal solutions, Ni and Mn exhibited the lowest current densities at −1 V, suggesting they are rate-limiting during alloy deposition. The slow deposition rate of Mn is consistent with the high overpotential required for its reduction at pH 2, as indicated in its Pourbaix diagram. In contrast, the Pourbaix diagram for Ni does not suggest similarly hindered deposition, implying that kinetic or complexation effects may also play a role in its reduced current density.

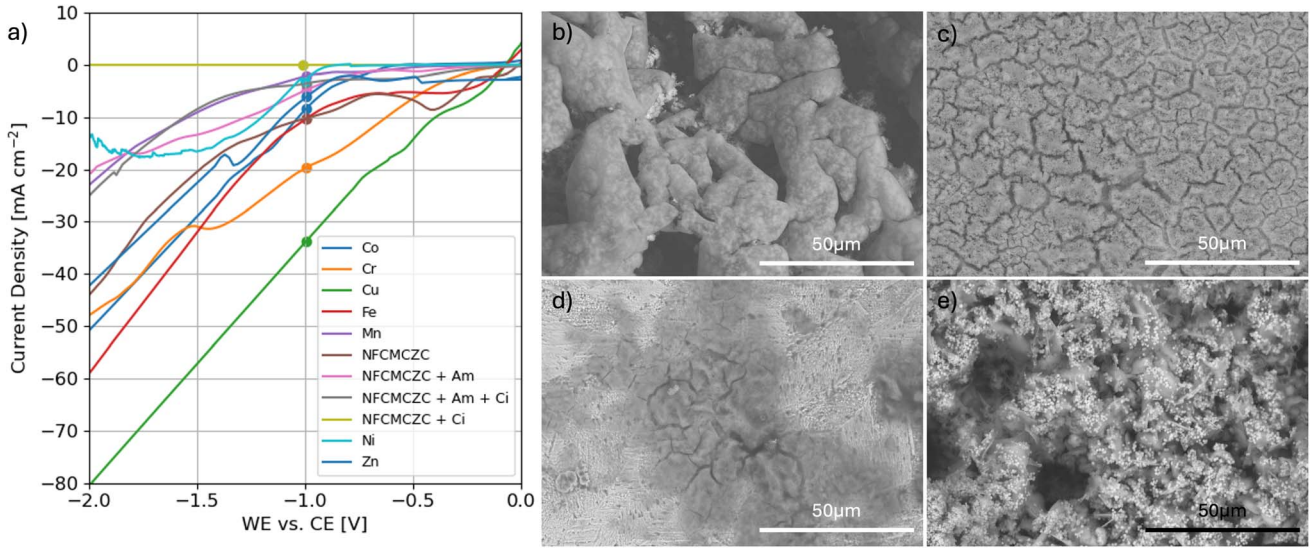

Fig. 5 (a) CV showing the current response of individual metal solutions and their combinations, with and without complexing agents. Full CV in SI Fig. S16. (b–e) SEM images of electrodeposited surfaces of NFCMCZC mixtures: (b) with both sodium citrate and ammonium hydroxide (Ci + Am), (c) with sodium citrate only (Ci), (d) with ammonium hydroxide only (Am), (e) without any complexing agents.

Table 1 summarizes the approximated limiting current densities for individual metal solutions as well as for the combined NFCMCZC mixtures, both with and without complexing agents. Among the single-metal solutions, Cu exhibited the highest limiting current density of 33.68 mA cm^{-2}, followed by Cr and Fe. In contrast, Mn and Ni displayed the lowest values, with limiting current densities of 2.09 and 2.95 mA cm^{-2}, respectively, suggesting that these metals may be rate-limiting in alloy deposition.

The limiting current density of the unmodified NFCMCZC mixture (without complexing agents) was 10.18 mA cm^{-2}, a value that falls between those of its individual constituents. This suggests that a mixture exhibits a combined electrochemical behavior of the faster-depositing metals (*i.e.*, Cu, Cr, Fe) and slower-depositing metals (*i.e.*, Ni, Mn, Co).

The addition of complexing agents leads to a notable decrease in the limiting current. The effect is most pronounced when sodium citrate is used alone (0.00 mA cm^{-2}), effectively suppressing deposition under the tested conditions. When ammonium hydroxide is used alone, the limiting current density drops to 4.76 mA cm^{-2}, and further decreases to 3.56 mA cm^{-2} when both complexing agents are present. These findings align well with previous studies indicating that sodium ions suppress hydrogen evolution and retard deposition kinetics.[37] Moreover, To *et al.*[38] demonstrated that complexation with citrate and ammonium can moderate the release of metal ions into the solution, thereby reducing the deposition rate. This mechanistic interpretation is consistent with the observed trends in limiting current densities for the multi-metal mixtures.

Table 1 Approximated limiting current densities for individual metal solutions and NFCMCZC mixtures. The concentration of the stock solutions without the complexing agents was set to 0.4 M

Metal deposited	Limiting current density [mA cm^{-2}]
Ni	2.95
Fe	10.26
Cr	19.62
Mn	2.09
Co	8.32
Zn	6.11
Cu	33.68
NFCMCZC + Ci	0.00
NFCMCZC + Am	4.76
NFCMCZC + Ci + Am	3.56
NFCMCZC	10.18

3.3 Deposition behavior and compositional analysis

Scanning electron microscopy and energy dispersive X-ray spectroscopy (SEM-EDS) analyses were performed on samples electrodeposited from the NFCMCZC precursor solution to assess the influence of complexing agents on the resulting alloy composition. The deposition was conducted at a current density of 10 mA cm^{-2} for 60 seconds, using either no additive, one complexing agent, or a combination of ammonium hydroxide and sodium citrate. The measured elemental compositions were compared to the dispensed volume ratios of the precursors and additives, as summarized in Table 2.

The results suggest that metals tend to deposit more uniformly when either no complexing agents or both complexing agents are used. In contrast, using only one agent leads to nickel-dominated surfaces, with lower incorporation of the remaining metals. Represented SEM images of the NFCMCZC-deposited surfaces are shown in Fig. 5b–e. The most pronounced surface texture (presence of ridges, edges, and cavities) was observed when both complexing agents are used (Fig. 5b) or omitted entirely (Fig. 5e). These morphological

Table 2 Dispensed volume % of metal solutions and complexing agents compared to SEM-EDS elemental composition (%)

	Ni	Fe	Cr	Co	Mn	Cu	Zn	Am	Ci
Vol%	11	11	11	11	11	11	11	11	11
EDS%	42.4	4.2	0.2	13.3	0.3	34.5	5.3		
Vol%	13	13	13	13	13	13	13		13
EDS%	92	1	1.2	2	1.7	0	2.2		
Vol%	13	13	13	13	13	13	13	13	
EDS%	96.4	0.7	2.6	0	0.3	0	0		
Vol%	14	14	14	14	14	14	14		
EDS%	4.7	3.7	17.4	4.7	0.8	51.2	17.5		

features are desirable for electrocatalysts, as they increase surface area and expose edge sites likely to contribute to catalytic activity. In contrast, the samples after the electrodeposition with only one complexing agent exhibited smoother and more homogeneous surfaces, consisting mainly of Ni.

Analysis of 70 SEM-EDS images revealed notable variation in elemental distribution across the samples. However, metals were generally well dispersed. Exceptions were occasionally observed for Mn and Cu, which tended to form localized clusters. Representative EDS maps are provided in the SI (Fig. S13 and S14).

4 Showcase: alkaline oxygen evolution reaction catalysts

The capabilities of the AMPERE-2 platform were demonstrated through the synthesis and evaluation of OER catalysts in alkaline media. Catalyst films were deposited using the NFCMCZC precursor solution at a current density of 10 mA cm^{-2}. All OER measurements were performed in 1 M KOH at 35 °C without pre-electrolysis of the electrolyte, which may result in trace Fe contamination that can artificially enhance OER activity.[34]

Fig. 6 shows the average OER overpotential, measured at four different current densities (10, 20, 50, and 100 mA cm^{-2}), as a function of electrodeposition time. Ohmic correction (90% compensation) was applied, and values reflect the final 20 seconds of each CC measurement. The results indicate that the deposition times of 30–60 seconds yield the lowest overpotentials, suggesting an optimal balance between catalyst layer thickness and electrochemical performance. Longer deposition times do not improve activity further, likely due to increased resistance or passivation effects.

The influence of complexing agents on catalyst performance is illustrated in Fig. 7. CV curves show the OER behavior of catalysts synthesized with varying volumetric combinations of ammonium hydroxide and sodium citrate. Oxidation peaks appear around 1.6 V and 1.7 V *vs.* RHE. Samples synthesized with only sodium citrate as the complexing agent (dotted lines) exhibit higher OER potentials compared to those synthesized with ammonium hydroxide. Increasing the sodium citrate

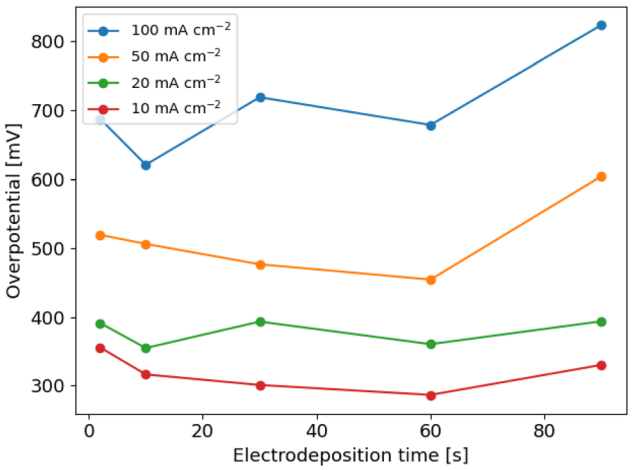

Fig. 6 Average OER overpotential at 10, 20, 50 and 100 mA cm^{-2}, measured on NFCMCZC + Am + Ci samples electrodeposited for different durations. Values reflect the final 20 seconds of each constant current step, corrected for 90% ohmic resistance.

content does not appear to affect performance significantly, while a small amount of ammonium hydroxide leads to notable improvements.

The lowest OER potential of the NFCMCZC alloy were observed when both complexing agents were used in equal amounts, yielding the overpotential at 20 mA cm^{-2} and 50 mA cm^{-2} to be $\eta_{20} = 408$ mV and $\eta_{50} = 497$ mV, respectively.

For comparison, benchmark catalysts were synthesized and tested under the same conditions. A $Ni_{0.5}Fe_{0.5}$ alloy exhibited the best performance, with OER overpotential of $\eta_{20} = 357$ mV and $\eta_{50} = 411$ mV, consistent with prior reports by Trotochaud *et al.*[39] and Youn *et al.*[40] ($\eta_{20} = 370$ mV). In contrast, another

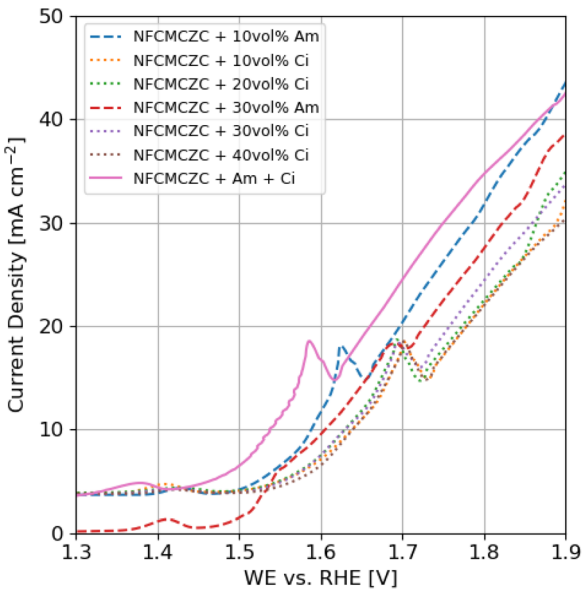

Fig. 7 Cyclic voltammetry of catalysts synthesized from NFCMCZC with different combinations of ammonium hydroxide and sodium citrate as complexing agents.

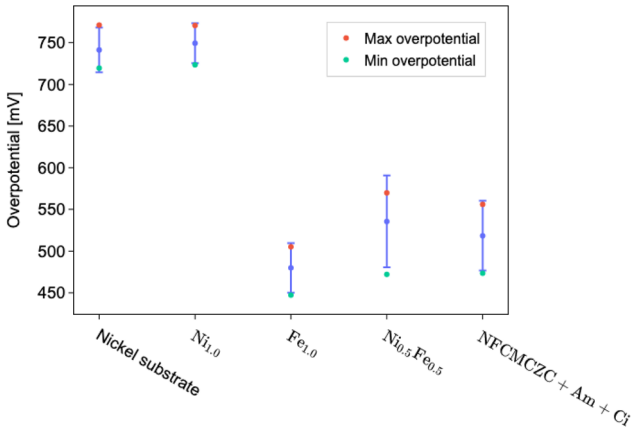

Fig. 8 Reproducibility of OER measurements across replicate catalyst samples, assessed by the variation in potential at 50 mA cm^{-2}. The blue dots represent the mean overpotential, error bars indicate the standard deviation, and the red and green markers denote the maximum and minimum values observed within each sample set.

benchmark sample NiO_x yielded significantly higher overpotential of approximately $\eta_{20} = 559$ mV and $\eta_{50} = 731$ mV, in line with literature values from Mccrory *et al.*[41] ($\eta_{20} = 510$ mV) and Lyu *et al.*[42] ($\eta_{10} = 433$ mV on nickel foam).

4.1 Reproducibility

To assess reproducibility, the OER potential at 50 mA cm^{-2} was measured for a range of catalyst compositions, including $Fe_{1.0}$, $Ni_{1.0}$, $Ni_{0.5}Fe_{0.5}$, and the NFCMCZC alloy with complexing agents, along with a bare nickel substrate as control. The standard deviations ranged from 24 mV to 55 mV, depending on the material composition (see Fig. 8). These results demonstrate consistent electrochemical performance across replicate samples, validating the reliability of the AMPERE-2 platform.

5 Conclusion

This study demonstrated the successful implementation of the AMPERE-2 platform for automated electrodeposition and electrochemical testing. The setup reliably employed metal chloride precursors for alloy deposition and enabled fully automated catalytic evaluation under alkaline conditions. The inclusion of complexing agents, ammonium hydroxide and sodium citrate, was found to influence both the deposition process and the resulting surface morphology. SEM analysis showed that catalysts prepared with either both complexing agents or none exhibited sponge-like textures and increased surface area, correlating with improved OER performance. In contrast, using a single complexing agent led to smoother surfaces with lower surface area and the presence of cracks.

Electrochemical testing revealed that deposition time strongly influences the catalytic activity, with optimal performance observed for deposition durations between 30 to 60 seconds. EDS analysis confirmed incorporation of all targeted metals, though the final composition deviated from the dispensed volume ratios. Reproducibility tests showed a variation in overpotential at 50 mA cm^{-2} ranging from 24 to 55 mV, depending on the composition. This work highlights the potential of an autonomous experimental platform like AMPERE-2 to accelerate materials discovery and improve reproducibility in catalyst development. By lowering technical and financial barriers, this approach contributes to the broader democratization of self-driving laboratories.

Author contributions

Contributions are defined here after CRediT (the Contributor Roles Taxonomy). Nis Fisker-Bødker: conceptualization, data curation, formal analysis, investigation, methodology, project administration, resources, software, validation, visualization, writing – original draft, writing – review and editing. Daniel Persaud: investigation, software, resources, validation, Yang Bai: investigation, resources, writing – review and editing, visualization, Mark Kozdras: conceptualization, methodology, Tejs Vegge: supervision, writing – review and editing, Funding acquisition, Jason Hattrick-Simpers: conceptualization, resources, funding acquisition, project administration, Jin Hyun Chang: supervision, writing – original draft, writing – review and editing.

Conflicts of interest

There are no conflicts of interest to declare.

Data availability

The complete AMPERE-2 workflow, which integrates both wrappers for automated electrodeposition and electrochemical testing, Labware files for the Opentron, as well as a complete list of components, 3D files, Arduino code and chemicals used in the platform, is available at DOI: **https://doi.org/10.5281/zenodo.15575908**.[43] This is the main SDL repository needed to replicate the setup. The Python wrapper for the Opentron OT-2, used to issue real-time commands and included in the SDL main repo, is available at DOI: **https://doi.org/10.5281/zenodo.15311179**.[44] The Python wrapper for the Admiral Squidstat potentiostat (also included in the SDL main repo) can be accessed at DOI: **https://doi.org/10.5281/zenodo.15575944**.[45] The 1454 datasets used as basis for this paper can be found at DOI: **https://doi.org/10.11583/DTU.27446925**.[46]

Supplementary information is available with images of the tools, setup, calibration method and data on the peristaltic pumps, the robotic workflow, SEM EDS images, electric diagram, list of materials, a full CV of limiting current scan and python install instructions. See DOI: **https://doi.org/10.1039/d5dd00180c**.

Acknowledgements

The authors gratefully acknowledge Rachel Keunen for her organizational support, assistance in resource coordination, and contributions to project management. We thank Eloise

Besnier for laboratory assistance and technical support, and Dian Yu for her dedicated contributions to experimental work. We acknowledge financial support from the Pioneer Center for Accelerating P2X Materials Discovery (CAPeX), DNRF grant number P3 at the Technical University of Denmark (DTU) through a Digital PhD scholarship, and the Independent Research Foundation Denmark (0217-00326B). This research was also undertaken in part thanks to funding provided to the University of Toronto Acceleration Consortium from the Canada First Research Excellence Fund (Grant number CFREF-2022-00042).

Notes and references

1 B. P. MacLeod, F. G. L. Parlane, T. D. Morrissey, F. Häse, L. M. Roch, K. E. Dettelbach, R. Moreira, L. P. E. Yunker, M. B. Rooney, J. R. Deeth, V. Lai, G. J. Ng, H. Situ, R. H. Zhang, M. S. Elliott, T. H. Haley, D. J. Dvorak, A. Aspuru-Guzik, J. E. Hein and C. P. Berlinguette, *Sci. Adv.*, 2020, **6**, 1–8.

2 F. Häse, L. M. Roch and A. Aspuru-Guzik, *Trends Chem.*, 2019, **1**, 282–291.

3 A. Dave, J. Mitchell, S. Burke, H. Lin, J. Whitacre and V. Viswanathan, *Nat. Commun.*, 2022, **13**, 5454.

4 J. Ruza, M. Stolberg, S. Cawthern, J. Johnson, Y. Shao-Horn and R. Gomez-Bombarelli, Autonomous Discovery of Polymer Electrolyte Formulations with Warm-start Batch Bayesian, *ChemRxiv*, 2025, 1–13, **https://chemrxiv.org/engage/chemrxiv/article-details/67e46e95fa469535b99df4ee**.

5 J. A. Bennett, N. Orouji, M. Khan, S. Sadeghi, J. Rodgers and M. Abolhasani, *Nat. Chem. Eng.*, 2024, **1**, 240–250.

6 M. B. Rooney, B. P. MacLeod, R. Oldford, Z. J. Thompson, K. L. White, J. Tungjunyatham, B. J. Stankiewicz and C. P. Berlinguette, *Digital Discovery*, 2022, **1**, 382–389.

7 G. Tom, S. P. Schmid, S. G. Baird, Y. Cao, K. Darvish, H. Hao, S. Lo, S. Pablo-García, E. M. Rajaonson, M. Skreta, N. Yoshikawa, S. Corapi, G. D. Akkoc, F. Strieth-Kalthoff, M. Seifrid and A. Aspuru-Guzik, *Chem. Rev.*, 2024, **124**, 9633–9732.

8 Q. Zhu, Y. Huang, D. Zhou, L. Zhao, L. Guo, R. Yang, Z. Sun, M. Luo, F. Zhang, H. Xiao, X. Tang, X. Zhang, T. Song, X. Li, B. Chong, J. Zhou, Y. Zhang, B. Zhang, J. Cao, G. Zhang, S. Wang, G. Ye, W. Zhang, H. Zhao, S. Cong, H. Li, L. L. Ling, Z. Zhang, W. Shang, J. Jiang and Y. Luo, *Nat. Synth.*, 2024, **3**, 319–328.

9 B. Zhang, Z. Zhu, H. Li, J. Cao and J. Jiang, *CCS Chem.*, 2025, **7**, 345–360.

10 A. Sanin, J. K. Flowers, T. H. Piotrowiak, F. Felsen, L. Merker, A. Ludwig, D. Bresser and H. S. Stein, *Adv. Energy Mater.*, 2025, **15**, 2404961.

11 B. Burger, P. M. Maffettone, V. V. Gusev, C. M. Aitchison, Y. Bai, X. Wang, X. Li, B. M. Alston, B. Li, R. Clowes, N. Rankin, B. Harris, R. S. Sprick and A. I. Cooper, *Nature*, 2020, **583**, 237–241.

12 P. J. Kitson, G. Marie, J.-P. Francoia, S. S. Zalesskiy, R. C. Sigerson, J. S. Mathieson and L. Cronin, *Science*, 2018, **359**, 314–319.

13 S. Back, A. Aspuru-Guzik, M. Ceriotti, G. Gryn'ova, B. Grzybowski, G. H. Gu, J. Hein, K. Hippalgaonkar, R. Hormázabal, Y. Jung, S. Kim, W. Y. Kim, S. M. Moosavi, J. Noh, C. Park, J. Schrier, P. Schwaller, K. Tsuda, T. Vegge, O. A. von Lilienfeld and A. Walsh, *Digital Discovery*, 2023, **3**, 23–33.

14 R. B. Canty, J. A. Bennett, K. A. Brown, T. Buonassisi, S. V. Kalinin, J. R. Kitchin, B. Maruyama, R. G. Moore, J. Schrier, M. Seifrid, S. Sun, T. Vegge and M. Abolhasani, *Nat. Commun.*, 2025, **16**, 3856.

15 E. Li, A. T. Lam, T. Fuhrmann, L. Erikson, M. Wirth, M. L. Miller, P. Blikstein and I. H. Riedel-Kruse, *PLoS One*, 2022, **17**, e0275688.

16 L. C. Gerber, A. Calasanz-Kaiser, L. Hyman, K. Voitiuk, U. Patil and I. H. Riedel-Kruse, *PLoS Biol.*, 2017, **15**, 1–9.

17 Y. Bai, Z. H. J. Khoo, R. I Made, H. Xie, C. Y. J. Lim, A. D. Handoko, V. Chellappan, J. J. Cheng, F. Wei, Y. F. Lim and K. Hippalgaonkar, *Adv. Mater.*, 2024, **36**, 2304269.

18 B. Pelkie, S. Baird, E. Aissi, K. Aspuru-Takata, Y. Cao, J. H. Chang, K. Gambhir, W. S. Hale, L. Hao, C. Hattrick, J. Hein, D. Luo, O. Melville, M. Ngan, L. L. B. Nyeland, N. Peek, M. Politi, E. E. Rajkumar, A. Siemenn, B. Subbaraman, S. Vasquez, J. Watchorn, W. Zhang, R. Ziskason, L. Pozzo, T. Buonassisi and T. Vegge, Democratizing self-driving labs through user-developed automation infrastructure, *ChemRxiv*, 2025, 1–18, **https://chemrxiv.org/engage/chemrxiv/article-details/67a4ffb6fa469535b94a3ad9**.

19 C. W. Coley, N. S. Eyke and K. F. Jensen, *Angew. Chem., Int. Ed.*, 2020, **59**, 23414–23436.

20 J. Abed, Y. Bai, D. Persaud, J. Kim, J. Witt, J. Hattrick-Simpers and E. H. Sargent, *Digital Discovery*, 2024, **3**, 2265–2274.

21 E. Fatehi, M. Thadani, G. Birsan and R. W. Black, A Critical Evaluation of a Self-Driving Laboratory for the Optimization of Electrodeposited Earth-Abundant Mixed-Metal Oxide Catalysts for the Oxygen Evolution Reaction (OER), *arXiv*, 2023, preprint, arXiv:2305.12541, DOI: **10.48550/arXiv.2305.12541**.

22 H. Sheng, J. Sun, O. Rodríguez, B. Hoar, W. Zhang, D. Xiang, T. Tang, A. Hazra, D. Min, A. Doyle, M. Sigman, C. Costentin, Q. Gu, J. Rodríguez-López and C. Liu, Autonomous closed-loop mechanistic investigation of molecular electrochemistry *via* automation, *ChemRxiv*, 2023, 1–20, **https://chemrxiv.org/engage/chemrxiv/article-details/651dec9545aaa5fdbb504964**.

23 H. Quinn, G. A. Robben, Z. Zheng, A. L. Gardner, J. G. Werner and K. A. Brown, PANDA: A self-driving lab for studying electrodeposited polymer films, *arXiv*, 2024, preprint, arXiv:2406.17725, DOI: **10.48550/arXiv.2406.17725**.

24 J. Qi, W. Zhang, R. Xiang, K. Liu, H. Wang, M. Chen, Y. Han and R. Cao, *Adv. Sci.*, 2015, **2**, 1–8.

25 H. Xiao, H. Shin and W. A. Goddard, *Proc. Natl. Acad. Sci. U. S. A.*, 2018, **115**, 5872–5877.

26 M. A. Ha, S. M. Alia, A. G. Norman and E. M. Miller, *ACS Catal.*, 2024, **14**, 17347–17359.

27 I. Vincent, E.-C. Lee and H.-M. Kim, *Catalysts*, 2022, **12**, 476.

28 N. Li, D. K. Bediako, R. G. Hadt, D. Hayes, T. J. Kempa, F. Von Cube, D. C. Bell, L. X. Chen and D. G. Nocera, *Proc. Natl. Acad. Sci. U. S. A.*, 2017, **114**, 1486–1491.
29 D. A. Corrigan, *J. Electrochem. Soc.*, 1987, **134**, 377–384.
30 H. Y. Jung, J. H. Park, J. C. Ro and S. J. Suh, *ACS Omega*, 2022, **7**, 45636–45641.
31 B. Hong, C. hai Jiang and X. jian Wang, *Surf. Coat. Technol.*, 2007, **201**, 7449–7452.
32 J. Wang, S. Liu, Y. Mu, L. Yang, J. Yang, S. Feng, M. Shi, W. Yang, W. Fu and H. Yang, *J. Alloys Compd.*, 2018, **748**, 515–521.
33 T. J. Whang, M. T. Hsieh and Y. C. Kao, *Appl. Surf. Sci.*, 2010, **257**, 1457–1462.
34 L. Liu, L. P. Twight, J. L. Fehrs, Y. Ou, D. Sun and S. W. Boettcher, *ChemElectroChem*, 2022, **9**, e202200279.
35 T. Lim, J. Kim and S. H. Joo, *J. Electrochem. Sci. Technol.*, 2023, **14**, 105–119.
36 C. Ponce-De-León, C. T. Low, G. Kear and F. C. Walsh, *J. Appl. Electrochem.*, 2007, **37**, 1261–1270.
37 K. E. Ferguson, PhD thesis, University of Nottingham, 1999.
38 D. T. To, S. H. Park, M. J. Kim, H.-S. Cho and N. V. Myung, *Front. Chem.*, 2022, **10**, 1–12.
39 L. Trotochaud, J. K. Ranney, K. N. Williams and S. W. Boettcher, *J. Am. Chem. Soc.*, 2012, **134**, 17253–17261.
40 D. H. Youn, Y. B. Park, J. Y. Kim, G. Magesh, Y. J. Jang and J. S. Lee, *J. Power Sources*, 2015, **294**, 437–443.
41 C. C. L. Mccrory, S. Jung, J. C. Peters and T. F. Jaramillo, *J. Am. Chem. Soc.*, 2013, S1–S32.
42 X. Lyu, J. Li, J. Yang and A. Serov, *J. Environ. Chem. Eng.*, 2023, **11**, 1–6.
43 N. Fisker-Bødker, *AMPERE-2 Workflow, Automated Electrodeposition and Electrochemical Testing*, 2025, DOI: **10.5281/zenodo.15575908**.
44 D. Persaud, *Python Wrapper for Opentrons OT-2*, 2025, DOI: **10.5281/zenodo.15311179**.
45 N. Fisker-Bødker, *Python Wrapper for Admiral Squidstat Potentiostat*, 2025, DOI: **10.5281/zenodo.15575944**.
46 N. Fisker-Bødker, *Dataset for Democratizing self-driving lab platform for electrodeposition of catalyst and electrochemical validation*, 2025, DOI: **10.11583/DTU.27446925**.